Kobe University Repository : Kernel

PDF issue: 2026-11-02

Differential disruption of autoinhibition and defect in assembly of cytoskeleton during cell division decide the fate of human DIAPH1-related cytoskeletopathy

Kim, Bong Jik ; Ueyama, Takehiko ; Miyoshi, Takushi ; Lee, Seungmin ; Han, Jin Hee ; Park, Hye-Rim ; Kim, Ah Reum ; Oh, Jayoung ; Kim, Min…

(Citation)
Journal of Medical Genetics,56(12):818-827

(Issue Date)
2019-12

(Resource Type)
journal article

(Version)
Accepted Manuscript

(Rights)
© Authors (or their employer(s)) 2019.
Reuse of this manuscript version (excluding any databases, tables, diagrams, photographs and other images or illustrative material included where a another copyright owner is identified) is permitted strictly pursuant to the terms of the…

(URL)
https://hdl.handle.net/20.500.14094/90008242

KOBE UNIVERSITY

DIFFERENTIAL DISRUPTION OF AUTOINHIBITION AND DEFECT IN ASSEMBLY OF CYTOSKELETON DURING CELL DIVISION DECIDE THE FATES OF HUMAN *DIAPH1*-RELATED CYTOSKELETOPATHY

Bong Jik Kim[1,2]†, Takehiko Ueyama[3]†*, Takushi Miyoshi[4]†, Seungmin Lee[2], Jin Hee Han[2], Hye-Rim Park[2], Ah Reum Kim[5], Jayoung Oh[2], Min Young Kim[2], Yong Seok Kang[2], Doo Yi Oh[2], Jiwon Yun[6,7], Sang Mee Hwang[6,7], Nayoung K.D. Kim[5,8], Woong-Yang Park[5,8], Shin-ichiro Kitajiri[9]*, Byung Yoon Choi[2,10]*

[1]Department of Otolaryngology-Head and Neck Surgery, Chungnam National University College of Medicine, Daejeon, Korea. [2]Department of Otorhinolaryngology-Head and Neck Surgery, Seoul National University Bundang Hospital, Seoul National University College of Medicine, Seongnam, Korea. [3]Laboratory of Molecular Pharmacology, Biosignal Research Center, Kobe University, Kobe 657-8501, Japan. [4]Department of Otolaryngology, Head and Neck Surgery, Graduate School of Medicine, Kyoto University, Kyoto 606-8507, Japan. [5]Samsung Genome Institute, Samsung Medical Center, Seoul, Korea. [6]Department of Laboratory Medicine, Seoul National University College of Medicine, Seoul, Korea. [7]Department of Laboratory Medicine, Seoul National University Bundang Hospital, Seongnam, Korea. [8]Department of Molecular Cell Biology, School of Medicine, Sungkyunkwan University, Seoul, Korea. [9]Department of Otorhinolaryngology, Shinshu University School of Medicine, Matsumoto 390-8621, Japan. [10]Sensory Organ Research Institute, Seoul National University Medical Research Center, Seoul, Korea.

†These authors contributed equally to this work
*These authors equally supervised this work.

Correspondence:

Takehiko Ueyama, MD, PhD,
Laboratory of Molecular Pharmacology, Biosignal Research Center, Kobe University, Rokkodai-cho 1-1, Nada-ku, Kobe 657-8501, Japan. Tel: +81-78-803-5962, Fax: +81-78-803-5971, E-mail: tueyama@kobe-u.ac.jp

Shin-ichiro Kitajiri, MD, PhD,
Department of Otorhinolaryngology, Shinshu University School of Medicine, 3-1-1 Asahi, Matsumoto, 390-8621, Japan. Tel: +81-263-37-2666, Fax: +81-263-36-9164, Email:kitajiri@shinshu-u.ac.jp

Byung Yoon Choi, MD, PhD,
Department of Otorhinolaryngology–Head & Neck Surgery, Seoul National University Bundang Hospital, 300 Gumi- dong, Bundang- gu, Seongnam 13620, Republic of South Korea. Tel: +82-31-787-7406, Fax: +82-31-787-4057, E-mail: choiby2010@gmail.com

ABSTRACT

Background: Diaphanous-related formins1 (DIA1), which assembles the unbranched actin microfilament and microtubule cytoskeleton, is encoded by *DIAPH1*. Constitutive activation by the disruption of autoinhibitory interactions between the N-terminal diaphanous inhibitory domain (DID) and C-terminal diaphanous auto regulatory domain (DAD) dysregulates DIA1, resulting in both hearing loss and blood cell abnormalities. **Methods and Results:** Here, we report the first constitutively active mutant in the DID (p.A265S) of humans with only hearing loss, and not blood cell abnormality through whole exome sequencing. The previously reported DAD mutants and our DID mutant (p.A265S) shared the finding of diminished autoinhibitory interaction, abnormally-upregulated actin polymerization activity, and increased localizations at the plasma membrane (PM). However, the obvious defect in the DIA1-driven assembly of cytoskeleton 'during cell division' was only from the DAD mutants, not from p.A265S, which did nor show any blood cell abnormality. We also evaluated the five DID mutants in the hydrophobic pocket since four of these five additional mutants were predicted to critically disrupt between the DID and DAD. These additional pathogenic DID mutants revealed varying degrees of defect in the DIA1-driven cytoskeleton assembly including nearly normal phenotype during cell division as well as obvious impaired autoinhibition, again coinciding with our key observation in DIA1 mutant (p.A265S) in the DID.

Conclusion: Here, we report the first mutant in the DID of humans with only hearing loss. The differential cell biological phenotypes of DIA1 during cell division appear to be potential determinants of the clinical severity of *DIAPH1*-related cytoskeletopathy in humans.

INTRODUCTION

DFNA1 [MIM: 124900] is the first non-syndromic, autosomal dominant deafness locus reported in the literature, which is caused by alterations of *DIAPH1* [1]. The *DIAPH1* gene encodes Diaphanous-related formins 1 (DIA1), which includes the GTPase binding domain (GBD), diaphanous inhibitory domain (DID), diaphanous autoregulatory domain (DAD), and formin homology domains (FH1 and FH2). These formins are known to efficiently assemble the unbranched/straight actin microfilament and microtubule cytoskeleton into certain architectures for several functions [2-4].

Interestingly, the pathogenic *DIAPH1* variants detected in the DAD, p.R1213X/p.R1204X and p.A1210S*fs*X31, have been shown to be associated with blood cell abnormalities, such as macrothrombocytopenia (MTC) and neutropenia, [5-7] as well as with hearing loss [5 8]. This suggests that DFNA1 is actually a syndromic disease. Specifically, DFNA1 due to p.R1213X has been reported to be associated with reduced proplatelet formation from the cultured megakaryocytes (MKs) cell as well as with increased filamentous actin and stable microtubules from the platelets [5 8]. This blood cell phenotype was even shown to be progressive [5-7].

Very recently, the main pathophysiologic mechanism of hearing loss and blood cell phenotypes related to the pathogenic *DIAPH1* variants was discovered to be the constitutive activation of DIA1 via molecular disruption of autoinhibitory interactions between the C-terminal DAD and N-terminal DID [8], which can be released by an interaction with GTP-bound Rho in physiological conditions [9]. Indeed, rigorously characterized DFNA1 mutants, p.R1213X/p.R1204X, p.A1210S*fs*X31, p.A1210G*fs*X31, and p.E1192_Q1220del were located in the DAD [5 8 10]. Furthermore, various morphological abnormalities in stereocilia and

subsequent progressive hair cell loss *in vivo* have been observed, accounting for hearing loss caused by DAD mutants of DIA1[8].

However, despite essential contribution of the DID to this crucial autoinhibitory function in DIA1, no pathogenic variants in *DIAPH1* ever resided in the DID. Furthermore, the exact critical cell biological mechanisms that lead to altered megakaryopoiesis and platelet cytoskeletal dysregulation due to constitutive activation of DIA1 have not been fully elucidated yet.

In our present study, we characterize the first human pedigree carrying a pathogenic allele in the DID of *DIAPH1* and propose that the differential degree of functional alteration in DIA1 in dividing cells accounts for the phenotypic variability of DFNA1.

METHODS

Human subjects and audiometric evaluation

All procedures in this study were approved by the Institutional Review Boards of Seoul National University Bundang Hospital (IRB-B-1007-105-402). Written informed consent was obtained from all subjects. In the case of minors, written informed consent was obtained from parents or guardians. One multiplex Korean family (SB206) with segregation of perilingual, bilaterally symmetrical, downsloping hearing loss in an autosomal dominant fashion was included in this study. Among the SB206 family members, six individuals participated in the study **(Figure 1A)**. Pure-tone audiometry was performed on III:4, II:2, II:1, III:1, III:2, and III:3 with the air and bone conduction thresholds obtained at frequencies of 250–8000 Hz, as previously described [11 12]. Pure-tone audiograms for the two affected individuals are presented (**Figures 1B)**. II:1 (Father) and III:4 (daughter) showed bilateral, severe, and symmetrical sensorineural hearing loss (SNHL). Both affected subjects denied significant progression of hearing loss over time.

SNHL was most prominent in mid-to-high frequencies, with the mean threshold level of low frequencies being the lowest. However, the degree of hearing loss was slightly different among family members, manifesting intrafamilial variability. Specifically, auditory rehabilitation by hearing aid was sufficient for II:1, while III:4 had cochlear implantation operation for successful speech development.

Genetic analysis

Exome sequencing from the proband SB206-400 was performed, and bioinformatics analyses were done, as previously described [13-15]. The obtained reads were mapped onto the UCSC hg19 reference genome assembly, employing Lasergene 14 software package (DNASTAR, Madison, WI, USA).

The global MAF was identified, looking up to 1000 Genomes, Exome Aggregation Consortium (ExAC), NHLBI Grand Opportunity Exome Sequencing Project (GO-ESP), and genome aggregation database (gnomAD). The allele frequency in ethnicity-matched controls was calculated by checking the candidate variants against the Korean Reference Genome Database (KRGDB) that consists of 1722 Korean individuals. In addition, the pathogenicity of each variant was predicted by the SIFT, PolyPhen-2, Mutation Taster and we excluded SNPs that did not coincide with the autosomal dominant pattern. The remaining candidate SNPs were validated in other family members (II:1, II:2, III:1, III:2, III:3) by Sanger sequencing and scores of PhyloP, GERP++, CADD, and REVEL were further pursued.

Plasmids

Human *DIAPH1* generates two kinds of isoforms derived from alternative splicing, *DIAPH1*-isoform 1 (*DIA1-1*) (NM_005219) (NP_005210) and *DIAPH1*-isoform 2 (*DIA1-2*) (NM_001079812) (NP_001073280): DIA1-2 lacks exon 2 consisting of 27 base pairs, resulting in 9 amino acids (aa) shorter isoforms than DIA1-1 [16]. As a result, the same variant can have a different nomenclature depending on the isoform, such as p.R1213X (NM_005219) [5] and p.R1204X (NM_001079812) [8].

To examine the function of DIA1-1 mutant, p.A265S, we made plasmids that expressed the AcGFP-tagged wild-type (WT) and various mutants of DIA1-1. Those included the p.R1213X and p.M1199D variants that made DIA1 constitutively active by inducing the disruption of the autoinhibitory DID-DAD interaction [8 17]. The former was detected in human patients, while the latter was a hypothetical variant not found in humans, which was included only as an extreme pathogenic control. The hydrophobic face of the DAD defined by the M^{1199}DxLLxxL^{1206} consensus sequence binds to a shallow hydrophobic groove on the DID [18 19]. The five hypothetical variants in the DID (p.I231T, p.I231R, p.L262T, p.L262E, and p.E273R) were chosen for additional expression vectors, based on the analysis of 3D structure of DID/DAD interface. Ile231 and Leu262 are hydrophobic residues that form the hydrophobic pocket on the DID together with Ala265 necessary for binding to the hydrophobic face of the DAD (**Figure S1**), while Glu273 was reported not to be associated with the DID-DAD interaction [17].

Pull-down assay

Purified GST-DID, GST-DID(A265S), GST-DID(I231T), GST-DID I231R), GST-DID(L262T), GST-DID(L262E), and GST-DID(E273R) proteins were obtained, as previously described [20].

For quantitative assessment of the immunoreactive band, ImageJ software (National Institutes of Health) was used.

Live cell imaging using fluorescence single-molecule speckle (SiMS) microscopy

Fluorescence SiMS microscopy was performed, as previously described [8 21]. The cells expressing a low amount of AcGFP-tagged DIA1 proteins were observed, illuminating restricted areas near the edges of the cells. The density of speckles showing directional movement was calculated for each cell, and normalized by the fluorescent intensity of the cell edge, which corresponds to expression levels of AcGFP-tagged DIA1 proteins.

Statistical analysis

All data are presented as the mean ± SEM. One-way ANOVA followed by Tukey's multiple comparisons test was performed using Prism 6.0 software (GraphPad); $P < 0.05$ was considered statistically significant.

RESULTS

Genetic diagnosis

After the initial filtering step, 14 variants from 13 known deafness genes were selected as candidate pathogenic variants for III:4 **(Supplementary Table S1)**.

Next, we excluded the variants residing in *SLC26A5*, *KCNQ1*, *OTOGL*, *MYO15A*, *LOXHD1*, and *TSPEAR,* which – if mutated – are known to cause hearing loss in autosomal recessive inheritance. Among the remaining variants, only c.G793T (p.A265S) of *DIAPH1*

(NM_005219) perfectly co-segregated with deafness in other family members (II:1, II:2, III:1, III:2, III:3), as documented by Sanger sequencing **(Figures 1A-C)**.

The p.A265 residue was highly conserved among several species down to *hydra* **(Figure 1D)** and absent from 1000 Genomes, ExAC, GO-ESP, gnomAD, and KRGDB, suggesting its pathogenic potential. The pathogenic potential of the p.A265S variant of *DIAPH1* was predicted to be highly deleterious, as suggested by *in silico* prediction softwares: SIFT, Polyphen2, Mutation Taster, PhyloP, GERP++, CADD, and REVEL, further supporting its pathogenic effect **(Supplementary Table S1 and Table 1)**. Given this, p.A265S can be classified as a likely pathogenic variant [22 23]. Variant information has been deposited in LOVD under variant ID 0000453012 (https://www.lovd.nl)

Normal blood cell phenotype of SB206

Given that previous reports elucidated the tight association between the analyzed DFNA1 variants and blood cell abnormalities – especially platelet abnormality [5-7 24], we also examined the blood cell phenotype of SB206, expecting a similar blood cell phenotype.

Interestingly, serial evaluation of the phenotype of blood cells, including platelets from both III:4 and II:1, revealed that the number, shape, and size of platelet, as well as the number of white blood cells and red blood cells were perfectly normal **(Figure S2)**. This result was in sharp contrast with the p.R1213X variant of *DIAPH1,* which was tightly associated with MTC and other blood cell abnormalities.

Diminished autoinhibitory DID-DAD interaction in DIA1(A265S)

Since p.A265 resides in the DID, which is a counterpart of the DAD in the intramolecular

autoinhibitory interaction of DIA1 [25], we suspected a disruption of the DID-DAD interaction in p.A265S.

The autoinhibitory DID-DAD interaction was significantly and statistically weaker in the assay using DID(A265S) than that using WT DID **(Figure 2A)**, suggesting that the p.A265S variant is pathogenic and most likely a constitutively active mutant. However, the DID-DAD interaction for autoinhibition in the DID (A265S) was still markedly stronger than those using either DAD(R1213X) or DAD(M1199D), possibly revealing the order of potential pathogenic and constitutive activities: p.A265S < p.1213X and p.M1199D **(Figure 2B).**

Enhanced phalloidin staining in AcGFP-DIA1(A265S)-expressing cells during non-dividing phase

Given the diminished autoinhibitory DID-DAD interaction in the DID(A265S), as shown by the pull-down assay, we aimed to test the pathogenic potential of DIA1(A265S) using HeLa cells during the non-dividing phase. Previously, our group reported that the plasma membrane (PM) localization of GFP-tagged DIA1 is one of the surrogate markers of constitutive active DIA1 or even pathogenic DIA1 [8].

In our present study, some – if not all – AcGFP-DIA1(A265S)-expressing cells showed PM localization in sharp contrast with no PM localization of WT AcGFP-DIA1, further indicating the pathogenic potential of AcGFP-DIA1 (A265S) **(Figures 3A-B)**. To explore the functional outcome of mutant DIA1 expressing cells, we performed phalloidin staining. Intriguingly, unlike AcGFP-DIA1, the cells expressing AcGFP-DIA1(A265S) and AcGFP-DIA1(R1213X) showed significantly enhanced phalloidin staining at the outlines of the cells compared with the surrounding non-expressing cells. Enhanced phalloidin staining at the outlines of the cells of

these two mutant proteins were similar (**Figure 3B)**. Additionally, AcGFP-DIA1(A265S) – but not AcGFP-DIA1 – showed a localization to the tips of filopodia **(Figure 3B inset)**.

Furthermore, AcGFP-DIA1(M1199D)-expressing cells showed markedly enhanced stress fiber formation, while none of the AcGFP-DIA1, AcGFP-DIA1(A265S), and AcGFP-DIA1(1213X) showed such finding (**Figure 3B)**. Such enhanced phalloidin staining was indicative of constitutive activity of these mutants in actin polymerization, and the cells with such enhanced phalloidin staining showed increased PM localization of AcGFP-DIA1 mutants.

To quantitatively show the PM localization of AcGFP-DIA1(A265S), AcGFP-DIA1(R1213X), and AcGFP-DIA1(M1199D), the number of cells showing either PM localization or dot-like localization near the PM of each AcGFP-DIA1 protein/total number of cells expressing each AcGFP-DIA1 protein was calculated as a percentage: the order was AcGFP-DIA1(M1199D) > AcGFP-DIA1(R1213X) > AcGFP-DIA1(A265S) > AcGFP-DIA1; however, there was no statistical difference between p.R1213X and p.M1199D **(Figure 3C)**.

Taken together, the hypothetical constitutively active mutant, p.M1199D, was the most active among p.A265S, p.R1213X, and p.M1199D, consistent with previous reports [8 17]. In addition, p.M1199D showed the strongest PM localization, suggesting that the pathogenic effect of these mutant DIA1 proteins may be associated with PM localization.

Abnormally-upregulated actin elongation activity of DIA1(A265S) molecules in living cells

Based on the constitutively active characteristics of AcGFP-DIA1(A265S), as shown in the pull-down assay and immunohistochemistry, we aimed to detect the abnormally-upregulated actin elongation/polymerization activity in living cells. Previous fluorescence single-molecule speckle (SiMS) microscopy study in living cells revealed that the directional movement shown in the

activated GFP-DIA1 molecules was based on their processive actin-polymerization activity [26]. In other words, a few directionally-moving speckles are observed in the cells expressing WT GFP-DIA1, and the frequency of moving speckles significantly increases after microinjection of active RhoA mutant [26]. We observed that the XTC cells expressed AcGFP-DIA1(A265S), WT AcGFP-DIA1, AcGFP-DIA1(R1213X), and AcGFP-DIA1(M1199D), respectively, using SiMS microscopy **(Figures 4A-D, Movies S1-S4)**.

Moving speckles were rarely observed in cells expressing AcGFP-DIA1 **(Figure 4A, Movie S1),** reflecting static balance via the autoinhibitory DID-DAD interaction. In contrast, directionally-moving speckles were the most frequently observed in cells expressing the hypothetical mutant, AcGFP-DIA1(M1199D) with significantly impaired DID-DAD interaction **(Figure 4D, Movie S4).** Moving speckles in AcGFP-DIA1(A265S) and another mutant control AcGFP-DIA1(R1213X) were not as frequently observed as those in AcGFP-DIA1(M1199D); however, they were more frequently observed than those in AcGFP-DIA1. The density of moving speckles seemed similar between cells expressing AcGFP-DIA1(A265S) and AcGFP-DIA1(R1213X) **(Figures 4B-C, Movies S2-3).**

For semi-quantitative comparison, the densities of moving speckles were determined in multiple cells, and normalized by their expression levels **(Figure 4E)**. The 18-fold increase in the density of directionally-moving speckles from p.A265S compared with WT was noted (p = 0.0014). However, the densities of the moving speckles between p.A265S and p.R1213X were calculated to be statistically similar ($P > 0.9999$).

Accumulation of AcGFP-DIA1(A265S) at the spindle and contractile ring and findings from other mutant DIA1 proteins during cell division phase

We examined the important aspects required for successful cell division, using HeLa cells expressing AcGFP-tagged WT and mutant DIA1 proteins: AcGFP, AcGFP-DIA1, AcGFP-DIA1(A265S), AcGFP-DIA1(R1213X), and AcGFP-DIA1(M1199D). While AcGFP alone was not accumulated either at the spindle or at the contractile ring even with enhanced phalloidin staining at the contractile ring **(Figure 5A)**, the cells expressing AcGFP-DIA1 showed an accumulation at the spindle, albeit not at the contractile ring **(Figure 5B)**. Notably, AcGFP-DIA1(A265S) was accumulated both at the spindle and contractile ring **(Figure 5C),** again reflecting the constitutively active characteristics and pathogenic potential. However, no definite PM localization of AcGFP-DIA1(A265S) was noted. Trafficking of murine DIA1 to the spindle [27] and contractile ring during cell division [28] were consistent with previous reports. Thus, AcGFP-DIA1(A265S) more easily moves to the target sites, such as the spindle and contractile ring, where DIA1 functions, than AcGFP-DIA1 (see **Figure 3B** showing targeting of AcGFP-DIA1(A265S) to the tips of filopodia). In contrast, the cells expressing known mutant controls, AcGFP-DIA1(R1213X) and AcGFP-DIA1(M1199D), showed strong PM localization and asymmetrical accumulation at the contractile ring **(Figures 5D-F)**. AcGFP-DIA1 (R1213X) was also accumulated at the spindle in the metaphase; however, many of the cells expressing AcGFP-DIA1(M1199D) were floating and dead in the metaphase and thus not accumulated at the spindle **(Figures 5G)**.

These findings were consistent with the significantly decreased expression levels of AcGFP-DIA1(M1199D) compared with AcGFP-DIA1, AcGFP-DIA1(A265S), and AcGFP(R1213X) **(Figure 3A).** Additionally, more physiological behaviors of AcGFP-DIA1(A265S) not accompanied by strong PM localization and asymmetrical accumulation at the contractile ring during cell division may also be compatible with normal blood cell phenotypes related to

294 p.A265S of DID in humans. To determine if this weaker pathogenicity of p.A265S of DID is
295 universal throughout all the DID residues related to the DID-DAD interaction, we examined five
296 additional variants in the DID, including the one (p.E273R) predicted to not be associated with
297 the DID-DAD interaction. In the pulldown assay, GST-I231T, GST-I231R, GST-L262T, and
298 GST-L262E — whose mutated residues are located in the binding surface of the DID against the
299 DAD — showed impaired binding to the DAD, except GST-E273R; the order of the binding
300 strength was as follows: I231R, L262E < I231T < A265S < L262T < E273R (**Figure S3**). In the
301 HeLa cells, AcGFP-DIA1(I231T), AcGFP-DIA1(I231R), and AcGFP-DIA1(L262E), but not
302 AcGFP-DIA1(L262T) or AcGFP-DIA1(E273R), showed enhanced phalloidin staining and PM
303 localization (**Figure S4**). Furthermore, AcGFP-DIA1(I231T), AcGFP-DIA1(I231R), and
304 AcGFP-DIA1(L262E), but not AcGFP-DIA1(L262T) or AcGFP-DIA1(E273R), were
305 accumulated at the contractile ring, which was also not observed in the controls (AcGFP and
306 AcGFP-DIA1) (**Figure S5** and **Figure 5**). Data regarding the accumulation of controls (AcGFP
307 and AcGFP-DIA1) and AcGFP-DIA1 mutants at the contractile ring was shown in the
308 cumulative bar graph (**Figure S5G)**. The p.I231T mutant, in which the hydrophobic Isoleucine
309 was changed into the hydrophilic and non-charged residue as in the change of p.A265S mutant,
310 showed the most phenotypic similarities with the p.A265S mutant among the additional variants
311 in the pull-down assay and cell biological studies in the non-dividing and dividing phase. The
312 p.I231R mutant, in which the hydrophobic Isoleucine was changed into the positively charged
313 residue, showed the greatest phenotypic similarities with the p.R1213X mutant in these three
314 kinds of assays. The p.L262T mutant, in which the hydrophobic Leucine was changed into the
315 hydrophilic but non-charged residue exactly the same as in the change of p.A265S mutant,
316 manifested milder but obvious impairment of the DID-DAD interaction [17] **(Figure S3B),**

likely leading to at least DFNA1, if it happens in a real human patient. Interestingly, it also showed neither enhanced phalloidin staining nor accumulation at the contractile ring, presumably leading to a normal blood cell phenotype in a real human patient.

DISCUSSION

Despite the indispensable contribution of the DID to the crucial autoinhibitory function in DIA1, none of the reported variants to date in *DIAPH1* resided in the DID. They had been detected exclusively in the domains of FH1, FH2, DAD, or just around it [1 8 13 29]. In this study, p.A265S located in the DID of *DIAPH1* was proposed as a causative pathogenic variant of hearing loss in SB206 after the rigorous filtering process of candidate variants obtained from exome sequencing. The HL-specific ACMG/AMP rules indicated that p.A265S is likely pathogenic [23].

Interestingly, the Ala265 residue, which corresponds to Ala256 in murine DIA1 (NP_031884), along with Leu172, Asn226, Asn227, Gln361, and Asn319 (NP_005210) has been predicted by 3D structural studies to contribute to highly conserved patch that forms a concave and surface representing the DID structure, which binds to an amphipathic helix of the DAD segment [18 30] **(Figure S1).** Furthermore, Met1199 in the conserved DAD core region (M^{1199}DxLLxxL^{1206}) makes an hydrophobic interaction between the hydrophobic pocket on the DID formed by Met225, Ile231, Leu262, and Ala265 [18]. Indeed, a point mutation in hydrophobic Ala265 into Asp (D), a hydrophilic and negatively charged residue, drastically decreased the DID-DAD interaction [17 31]. Our novel variant results in a change of Ala265 into Ser (S), a hydrophilic but non-charged residue, suggesting that the A265S mutant would be, if not as A265D, apparently pathogenic. Thus, even without functional data analysis, the results of

molecular modeling strongly suggest that the p.A265S mutant would be pathogenic by specifically impairing the DID-DAD interaction, which is crucial for DIA1 autoinhibition.

Our present study is particularly intriguing because we discovered a real family segregating the hypothetical variant that had been theoretically predicted – via a 3D-structural analysis more than a decade ago – to be devastating for protein function [17 18]. In accordance with the prediction, the DIA1(A265S) mutant showed the enhanced actin polymerization accompanied with the localizations at the PM and filopodia tips in the transfected cells, diminished the autoinhibitory DID-DAD interaction as detected by pull-down assay, and abnormally upregulated the actin polymerization activity as detected by SiMS. This clearly suggests that p.A265S is pathogenic and entitles this variant to be the first DFNA1 variant detected from the DID. This tendency was further confirmed in experiments using the hypothetical DID variants harboring Ile231 and Leu262 residues critical for the DID-DAD interaction just like the Ala265 residue as predicted by the 3D structural analysis. Interestingly, recently published 'variant interpretation guidelines for genetic hearing loss' curated by the expert panel postulated that the phenotype of *DIAPH1*-related hearing loss is autosomal dominant hearing loss with macrothrombocytopenia [23]. Without rigorous functional analysis, the postulate may have jeopardized our hypothesis that p.A265S of *DIAPH1* is the cause of hearing loss in SB206, since macrothrombocytopenia was not observed from SB206.

We had previously reported that the PM localization of DIA1 is one of the surrogate markers of active or pathogenic DIA1 based on the results obtained from confocal microscopic studies and SiMS experiments [8]. In the previous study, we consistently showed that DIA1 (R1213X)/ DIA1(R1204X) is a constitutively active mutant, but definitely milder than DIA1(M1199D). Herein, PM localization – both in the dividing and non-dividing phases of cells

– and impairment of the DID-DAD interaction were significantly more prominent in p.R1213X than in p.A265S.

Intriguingly, p.R1213X/p.R1204X, p.A1210S*fs*X31, p.A1210G*fs*X31, and p.E1192_Q1220del, the main DFNA1 mutants, both showed their pathogenic potential, suggesting an association with blood cell abnormalities, like MTC [5-7 10]. The disrupted DID-DAD interaction and reduced proplatelet formation from cultured MKs was previously reported for p.R1213X [5 8]. The first reported DFNA1 variant, c.3661+1G>T, [1] has not been reported to cause MTC. However, this DFNA1 variant affected the residues downstream to the DAD, raising the possibility of being irrelevant to the disrupted DID-DAD interaction. The two missense variants, p.P678S in the FH1 domain [13] and p.I530S in the coiled-coil domain [32] of *DIAPH1* have been reported; however, the pathogenic potential of these variants remain somewhat elusive, and the blood cell phenotype was not evaluated in their reports. Therefore, the p.A265S variant may be the first and only pathogenic DFNA1 variant that is confirmed not to accompany the blood cell phenotype, indicating non-syndromic sensorineural hearing loss.

This less severe phenotype, which is related to p.A265S, compared with the phenotype previously reported for DFNA1mutants, such as p.R1213X/p.R1204X and p.A1210S*fs*X31, is supported by the quantitative data where the degree of PM localization and disruption of DAD-DID interaction by p.A265S is significantly milder than those of p.R1213X. However, the degree of hearing loss between the two variants (p.A265S vs p.R1213X) did not seem different. The pathogenic outcomes resulting from the disrupted DID-DAD interaction and prominent PM localization, if they go beyond a certain point, may have a ceiling effect, especially in non-dividing cells, such as the inner ear hair cells, leading to a similar hearing status with p.A265S and p.R1213X.

In contrast, the effect appears to be manifested more sensitively in a dose-dependent manner from the cells in the dividing phase; and more diverse findings, such as asymmetric accumulation of DIA1 mutants (p.R1213X and p.M1199D) at the contractile ring, were observed in the dividing phase of the cells. Therefore, these biological differences of the cells may become evident and manifested phenotypically only through the blood cells going through frequent cell division [5-7 33]. Unlike the major cells in the inner ear, such as hair cells and spiral ganglion cells that are related to hearing function and are fundamentally unable to proliferate or regenerate after birth, blood cells can divide, resulting in a much shorter lifespan. For example, the lifespans of platelets, neutrophils, and erythrocytes are 8~10 days [34], 8 hours to 5.4 days [35], and approximately 120 days [36], respectively. This information suggests that cell division is at least one of the important candidate steps that, if altered, can account for the phenotypes of blood cells in DFNA1 patients. Indeed, we observed different, but more physiological, behaviors of p.A265S during cell division compared with p.R1213X and p.M1199D, which was consistent with non-syndromic feature of p.A265S-based DFNA1. Previously, the essential role of murine DIA2 at the cleavage furrow/contractile ring during cytokinesis of proerythroblasts was reported [37]. Therefore, our results suggest that the abnormal and significantly dysregulated PM localization of DIA1 mutants (p.R1213X and p.M1199D) at the metaphase disturbs homeostatic cytokinesis of blood cells, which may be coordinated by DIA1 and DIA2. To evaluate whether the less severe disruption of cytoskeletal assembly during cell division related to the p.A265S mutant is universal throughout the DID residues involving the DID-DAD interaction, we examined five additional variants in the DID (p.I231T, p.I231R, p.L262T, p.L262E, and p.E273R), including the one (p.E273R) predicted not to be associated with the DID-DAD interaction. As expected, the four additional variants that were predicted to significantly affect

409 the DID-DAD interaction by 3D modeling showed variable degrees of impairment of the DID-
410 DAD interaction; this further supports our hypothesis that DID mutants could cause DFNA1.
411 Interestingly, the four additional DID mutants affecting the DID-DAD interaction showed a wide
412 phenotypic spectrum with respect to the defect in cytoskeleton assembly during cell division.
413 The p.L262T mutant showed no defect, while the p.I231R mutant manifested the most severe
414 defect, comparable to p.R1213X in the DAD domain. The degree of dysregulated cytoskeleton
415 assembly of p.I231T and p.L262E fell between them, the cell biological phenotype of p.I231T
416 being most similar to that of p.A265S. Our results suggest that the absence of blood cell
417 phenotypes in the DID mutants depends on the mutated sites and changed residues of the DID,
418 which led to a differential degree of defect in cytoskeleton assembly during cell division.
419 In the present study, there was a paradox: the SiMS experiments and phalloidin staining
420 suggested that DIA1(A265S) and DIA1(R1213X) are similarly constitutively active, while the
421 results from the pull-down assay, PM localization, and cell division-phase data suggested a
422 milder pathogenic potential of DIA1(A265S) than DIA1(R1213X). Which should we rely more
423 on to correlate with clinical findings? The PM localization of DIA1(R1213X) and
424 DIA1(M1199D) were much more prominent than that of DIA1(A265S), even in the SiMS
425 experiments **(Figure 4)**. To quote, DIA1 molecules with the released inhibitory DID-DAD
426 interaction likely have an "open" conformation, which possibly facilitates binding to actin
427 through the FH1 domain [30] and/or interaction with the PM [25]. Our speculation is that DIA1
428 mutant molecules located at the PM have strongly disrupted the DID-DAD interaction, thereby
429 obtaining more pathogenic conformation and activity than those located in the cytosol. However,
430 the SiMS experiments evaluate the linear actin polymerization activity of DIA1 molecules only
431 localized in the cytosol, indicating that the activity of DIA1 localized at the PM is unable to be

faithfully measured by SiMS. Thus, through the SiMS experiments, we probably failed to properly assess the difference in constitutive activity between the two mutants (DIA1(A265S) vs DIA1(R1213X)) with a different clinical severity. Therefore, a clear difference in blood cell phenotypes between DIA1(A265S) and DIA1(R1213X) may be better explained by the degree of PM localization.

Taken together, our data obtained by the confocal microscopic study both in dividing and non-dividing cells, as well as the pull-down assay and SiMS experiments indicated that the DIA1(A265S) mutant is the constitutively active mutant of DIA1, along with DIA1(R1213X) and DIA1(M1199D), making p.A265S to be the first variant residing in the DID of *DIAPH1*. Non-syndromic feature related to p.A265S was consistent with relatively milder findings in dividing cells, indicating that p.A265S may be the first real non-syndromic DFNA1 variant that went through a rigorous study. Thus, we, for the first time in literature, elucidated that the differential dysregulation of DIA1 during the cell division phase can lead to the manifestation of different phenotypes *in vitro*. Further, we also showed the presence of obvious defect in DIA1-driven assembly of cytoskeleton during cell division as a potential key determinant the clinical severity of *DIAPH1*-related cytoskeletopathy in humans.

Author's contributions: B.J.K., S.K., T.U. and B.Y.C. conceived and designed the experiments. Experiments were performed by T.M., J.H.H., J.O. M.Y.K., and T.U. Data analyses including bioinformatics analysis was performed by B.J.K., S.K., T.M., J.H.H., A.R.K., J.O., D.Y.O., N.K.D.K., T.U. and B.Y.C. Clinical data was analyzed by B.J.K., H.-R.P., J.Y., S.M.H., and Y.S.K. Supplementary figure was generated by S.L. Administrative assistance was provided by

H.-R.P. The manuscript was written by B.J.K., S.K., T.M., T.U., and B.Y.C., and critically reviewed by W.-Y.P. All authors contributed to the final manuscript.

Acknowledgments

We would like to give special thanks to Dr. Naoki Watanabe who generously allowed us to use his SiMS equipment.

Funding

This research was supported by the Basic Science Research Program through the National Research Foundation of Korea (NRF) funded by the Ministry of Education (2018R1A2B2001054 to B.Y.C.) and a grant of the Korea Health Technology R&D Project through the Korea Health Industry Development Institute (KHIDI), funded by the Ministry of Health & Welfare, Republic of Korea (grant numbers: HI15C1632, HI17C0952 to B.Y.C.). This research was partly supported by the grant from the Naito Foundation (to T.U.). The funders had no role in the study design, data collection and analysis, decision to publish, or preparation of the manuscript.

Conflict of Interest

The authors declare no conflict of interest.

References

1. Lynch ED, Lee MK, Morrow JE, et al. Nonsyndromic deafness DFNA1 associated with mutation of a human homolog of the Drosophila gene diaphanous. Science 1997;**278**(5341):1315-8
2. Chesarone MA, DuPage AG, Goode BL. Unleashing formins to remodel the actin and microtubule cytoskeletons. Nat Rev Mol Cell Biol 2010;**11**(1):62-74 doi: 10.1038/nrm2816[published Online First: Epub Date]|.
3. Goode BL, Eck MJ. Mechanism and function of formins in the control of actin assembly. Annu Rev Biochem 2007;**76**:593-627 doi: 10.1146/annurev.biochem.75.103004.142647[published Online First: Epub Date]|.
4. Wallar BJ, Alberts AS. The formins: active scaffolds that remodel the cytoskeleton. Trends Cell Biol 2003;**13**(8):435-46 doi: S0962892403001533 [pii][published Online First: Epub Date]|.
5. Stritt S, Nurden P, Turro E, et al. A gain-of-function variant in DIAPH1 causes dominant macrothrombocytopenia and hearing loss. Blood 2016;**127**(23):2903-14 doi: 10.1182/blood-2015-10-675629[published Online First: Epub Date]|.
6. Ganaha A, Kaname T, Shinjou A, et al. Progressive macrothrombocytopenia and hearing loss in a large family with DIAPH1 related disease. Am J Med Genet A 2017;**173**(10):2826-30 doi: 10.1002/ajmg.a.38411[published Online First: Epub Date]|.
7. Neuhaus C, Lang-Roth R, Zimmermann U, et al. Extension of the clinical and molecular phenotype of DIAPH1-associated autosomal dominant hearing loss (DFNA1). Clin Genet 2017;**91**(6):892-901 doi: 10.1111/cge.12915[published Online First: Epub Date]|.
8. Ueyama T, Ninoyu Y, Nishio SY, et al. Constitutive activation of DIA1 (DIAPH1) via C-terminal truncation causes human sensorineural hearing loss. EMBO Mol Med 2016;**8**(11):1310-24 doi: 10.15252/emmm.201606609[published Online First: Epub Date]|.
9. Amano M, Nakayama M, Kaibuchi K. Rho-kinase/ROCK: A key regulator of the cytoskeleton and cell polarity. Cytoskeleton (Hoboken) 2010;**67**(9):545-54 doi: 10.1002/cm.20472[published Online First: Epub Date]|.
10. Westbury SK, Downes K, Burney C, et al. Phenotype description and response to thrombopoietin receptor agonist in DIAPH1-related disorder. Blood Adv 2018;**2**(18):2341-46 doi: 10.1182/bloodadvances.2018020370[published Online First: Epub Date]|.
11. Kim SY, Kim AR, Kim NK, et al. Strong founder effect of p.P240L in CDH23 in Koreans and its significant contribution to severe-to-profound nonsyndromic hearing loss in a Korean pediatric population. J Transl Med 2015;**13**:263 doi: 10.1186/s12967-015-0624-8[published Online First: Epub Date]|.
12. Kim BJ, Kim AR, Park G, et al. Targeted Exome Sequencing of Deafness Genes After Failure of Auditory Phenotype-Driven Candidate Gene Screening. Otol Neurotol 2015;**36**(6):1096-102 doi: 10.1097/MAO.0000000000000747[published Online First: Epub Date]|.
13. Baek JI, Oh SK, Kim DB, et al. Targeted massive parallel sequencing: the effective detection of novel causative mutations associated with hearing loss in small families. Orphanet J Rare Dis 2012;**7**:60 doi: 1750-1172-7-60 [pii]
10.1186/1750-1172-7-60[published Online First: Epub Date]|.

14. Choi BY, Park G, Gim J, et al. Diagnostic application of targeted resequencing for familial nonsyndromic hearing loss. PLoS One 2013;**8**(8):e68692 doi: 10.1371/journal.pone.0068692 PONE-D-13-10680 [pii][published Online First: Epub Date]|.
15. Park G, Gim J, Kim AR, et al. Multiphasic analysis of whole exome sequencing data identifies a novel mutation of ACTG1 in a nonsyndromic hearing loss family. BMC genomics 2013;**14**:191 doi: 10.1186/1471-2164-14-191[published Online First: Epub Date]|.
16. Ueyama T. Rho-Family Small GTPases: From Highly Polarized Sensory Neurons to Cancer Cells. Cells 2019;**8**(2) doi: 10.3390/cells8020092[published Online First: Epub Date]|.
17. Lammers M, Rose R, Scrima A, et al. The regulation of mDia1 by autoinhibition and its release by Rho*GTP. Embo j 2005;**24**(23):4176-87 doi: 10.1038/sj.emboj.7600879[published Online First: Epub Date]|.
18. Nezami AG, Poy F, Eck MJ. Structure of the autoinhibitory switch in formin mDia1. Structure 2006;**14**(2):257-63 doi: 10.1016/j.str.2005.12.003[published Online First: Epub Date]|.
19. Wallar BJ, Stropich BN, Schoenherr JA, et al. The basic region of the diaphanous-autoregulatory domain (DAD) is required for autoregulatory interactions with the diaphanous-related formin inhibitory domain. J Biol Chem 2006;**281**(7):4300-7 doi: 10.1074/jbc.M510277200[published Online First: Epub Date]|.
20. Ueyama T, Tatsuno T, Kawasaki T, et al. A regulated adaptor function of $p40^{phox}$: distinct $p67^{phox}$ membrane targeting by $p40^{phox}$ and by $p47^{phox}$. Mol Biol Cell 2007;**18**(2):441-54 doi: 10.1091/mbc.E06-08-0731[published Online First: Epub Date]|.
21. Watanabe N. Fluorescence single-molecule imaging of actin turnover and regulatory mechanisms. Methods in enzymology 2012;**505**:219-32 doi: 10.1016/B978-0-12-388448-0.00020-6[published Online First: Epub Date]|.
22. Richards S, Aziz N, Bale S, et al. Standards and guidelines for the interpretation of sequence variants: a joint consensus recommendation of the American College of Medical Genetics and Genomics and the Association for Molecular Pathology. Genet Med 2015;**17**(5):405-24 doi: 10.1038/gim.2015.30[published Online First: Epub Date]|.
23. Oza AM, DiStefano MT, Hemphill SE, et al. Expert specification of the ACMG/AMP variant interpretation guidelines for genetic hearing loss. Hum Mutat 2018;**39**(11):1593-613 doi: 10.1002/humu.23630[published Online First: Epub Date]|.
24. Pan J, Lordier L, Meyran D, et al. The formin DIAPH1 (mDia1) regulates megakaryocyte proplatelet formation by remodeling the actin and microtubule cytoskeletons. Blood 2014;**124**(26):3967-77 doi: 10.1182/blood-2013-12-544924[published Online First: Epub Date]|.
25. Kuhn S, Geyer M. Formins as effector proteins of Rho GTPases. Small GTPases 2014;**5**:e29513 doi: 10.4161/sgtp.29513[published Online First: Epub Date]|.
26. Higashida C, Miyoshi T, Fujita A, et al. Actin polymerization-driven molecular movement of mDia1 in living cells. Science 2004;**303**(5666):2007-10 doi: 10.1126/science.1093923[published Online First: Epub Date]|.
27. Kato T, Watanabe N, Morishima Y, et al. Localization of a mammalian homolog of diaphanous, mDia1, to the mitotic spindle in HeLa cells. J Cell Sci 2001;**114**(Pt 4):775-84

28. Watanabe N, Madaule P, Reid T, et al. p140mDia, a mammalian homolog of Drosophila diaphanous, is a target protein for Rho small GTPase and is a ligand for profilin. EMBO J 1997;**16**(11):3044-56 doi: 10.1093/emboj/16.11.3044[published Online First: Epub Date]|.
29. Al-Maawali A, Barry BJ, Rajab A, et al. Novel loss-of-function variants in DIAPH1 associated with syndromic microcephaly, blindness, and early onset seizures. American journal of medical genetics Part A 2016;**170**(2):435-40 doi: 10.1002/ajmg.a.37422[published Online First: Epub Date]|.
30. Nezami A, Poy F, Toms A, et al. Crystal structure of a complex between amino and carboxy terminal fragments of mDia1: insights into autoinhibition of diaphanous-related formins. PloS one 2010;**5**(9) doi: 10.1371/journal.pone.0012992[published Online First: Epub Date]|.
31. Otomo T, Otomo C, Tomchick DR, et al. Structural basis of Rho GTPase-mediated activation of the formin mDia1. Mol Cell 2005;**18**(3):273-81 doi: S1097-2765(05)01226-8 [pii]
10.1016/j.molcel.2005.04.002[published Online First: Epub Date]|.
32. Kang TH, Baek JI, Sagong B, et al. A novel missense variant in the DIAPH1 gene in a Korean family with autosomal dominant nonsyndromic hearing loss. Genes Genet Syst 2017;**91**(5):289-92 doi: 10.1266/ggs.16-00041[published Online First: Epub Date]|.
33. Bastida JM, Lozano ML, Benito R, et al. Introducing high-throughput sequencing into mainstream genetic diagnosis practice in inherited platelet disorders. Haematologica 2018;**103**(1):148-62 doi: 10.3324/haematol.2017.171132[published Online First: Epub Date]|.
34. McArthur K, Chappaz S, Kile BT. Apoptosis in megakaryocytes and platelets: the life and death of a lineage. Blood 2018;**131**(6):605-10 doi: 10.1182/blood-2017-11-742684[published Online First: Epub Date]|.
35. Pillay J, den Braber I, Vrisekoop N, et al. In vivo labeling with 2H2O reveals a human neutrophil lifespan of 5.4 days. Blood 2010;**116**(4):625-7 doi: 10.1182/blood-2010-01-259028[published Online First: Epub Date]|.
36. Shah S, Huang X, Cheng L. Concise review: stem cell-based approaches to red blood cell production for transfusion. Stem Cells Transl Med 2014;**3**(3):346-55 doi: 10.5966/sctm.2013-0054[published Online First: Epub Date]|.
37. Watanabe S, De Zan T, Ishizaki T, et al. Loss of a Rho-regulated actin nucleator, mDia2, impairs cytokinesis during mouse fetal erythropoiesis. Cell Rep 2013;**5**(4):926-32 doi: 10.1016/j.celrep.2013.10.021[published Online First: Epub Date]|.

Figure legends

Fig. 1. A novel *DIAPH1* variant residing in the DID.

(A) Autosomal dominantly inherited sensorineural hearing loss (SNHL) is documented in a family (SB206). Black: affected, White: unaffected, M: male, F: female. Numbers represent the age at tested.

(B) The degree of hearing loss in II:1 (father) and III:4 (daughter) is severe SNHL and profound SNHL, respectively.

(C) The p.A265S variant perfectly co-segregates with the SNHL phenotype among the six (two affected and four unaffected) members of family SB206.

(D) The p.A265 residue is well conserved among the various species down to Hydra.

Fig. 2. Diminished and disrupted DID-DAD interaction by p.A265S, p.R1213X, and p.M1199D, respectively.

(A) Purified GST-tagged DID proteins (WT or p.A265S) were mixed with synthesized biotin-labeled DAD peptides (WT, p.R1213X, or p.M1199D) in a binding buffer. After rotation, streptavidin-coupled magnetic beads were added to the solution, and the mixture was agitated. The materials absorbed to the beads were subjected to SDS-PAGE, followed by immunoblotting using an HRP-conjugated GST antibody. Note the significantly diminished binding between DID(A265S) and WT DAD, disrupted bindings between WT DID and DAD(R1213X), as well as between WT DID and DAD(M1199D), compared with that between WT DID and WT DAD. Comparable levels of input (GST proteins) are shown in the left side of the panel. Representative of 7 experiments.

(B) The DID-DAD interaction was quantified using an ImageJ software (n=7, ****$P < 0.0001$ by one-way ANOVA followed by Tukey's *post hoc* test).

Fig. 3. Increased, but not as significant as in known constitutively active mutants, PM localization and enhanced phalloidin staining in AcGFP-DIA1(A265S) expressing HeLa cells.

AcGFP-DIA1, AcGFP-DIA1(A265S), AcGFP-DIA1(R1213X), and AcGFP-DIA1(M1199D) were transfected into HeLa cells.

(A) Forty-eight hours after transfection, the cell lysates were subjected to SDS-PAGE, followed by immunoblotting using an HRP-conjugated GFP antibody. Comparable loading of proteins is confirmed using an HRP-conjugated GAPDH antibody and expression levels of AcGFP-DIA1 (M1199D) was significantly decreased. Representative of 3 experiments.

(B) AcGFP-DIA1(A265S), but not WT AcGFP-DIA1, shows weak plasma membrane (PM) localization (arrowheads). The localization of AcGFP-DIA1(A265S) at the tips of filopodia is shown by arrows in the magnified image of the region indicated by the rectangle. AcGFP-DIA1(M1199D), but neither AcGFP-DIA1(A265S) nor AcGFP-DIA1(R1213X)-expressing cells show markedly enhanced stress fiber formation (asterisks). In contrast, AcGFP-DIA1(A265S) and AcGFP-DIA1(R1213X)-expressing cells show enhanced phalloidin staining at the outlines of the cells (circles). AcGFP-DIA1(R1213X) and AcGFP-DIA1(M1199D)-expressing cells show apparent PM localization (arrows). Scale bars: 10 μm.

(C) The graph demonstrates the percentage of cells showing PM localization or dot-like localization near the PM (from 3 independent experiments, ****$P < 0.0001$ by one-way ANOVA followed by Tukey's *post hoc* test).

Fig. 4. Abnormal actin elongation activity of mutant DIA1 molecules in living cells.

Directional movement of activated DIA1 molecules was visualized using fluorescence SiMS microscopy. Representative 300ms time-lapse images of XTC cells expressing AcGFP-tagged WT DIA1, DIA1 (A265S), DIA1 (R1213X), and DIA1(M1199D) were shown. **(A–D)** Directional movements of activated DIA1 molecules were indicated by circles and trajectories. The ends of the movements were shown by the crosses. Activated DIA1 molecules were the most frequent in cells expressing AcGFP-DIA1(M1199D), followed by AcGFP-DIA1(A265S) and AcGFP-DIA1(R1213X). A few activated molecules were observed in the cells expressing WT AcGFP-DIA1. Time is in seconds. Scale bars are 5 μm. Movies are shown by supplemental data (Movies S1–S4). **(E)** The frequency of activated DIA1 molecules was compared quantitatively between WT and mutants. The density of directionally-moving speckles were calculated and normalized by the fluorescent intensity of cell edge, which reflects the expression level of AcGFP-tagged DIA1 protein (WT: n = 5; A265S: n = 5; R1213X: n = 4; M1199D: n = 5). Statistical analysis by one-way ANOVA showed $P < 0.0001$. Post-hoc Tukey's multiple comparison test showed **$P = 0.0014$ (WT vs. A265S), *$P = 0.0271$ (A265S vs. M1199D), and $P > 0.9999$ (*N.S.*, A265S vs. R1213X).

Fig. 5. Accumulation of AcGFP-DIA1(A265S) at the spindle and contractile ring during cell division.

AcGFP, AcGFP-DIA1, AcGFP-DIA1(A265S), AcGFP-DIA1(R1213X), and AcGFP-DIA1(M1199D) were transfected into the HeLa cells. Thirty hours after transfection, the cells were fixed and stained using Alexa568-conjugated phalloidin (red) and DAPI (blue). Arrows and double arrows indicate accumulation at the spindle and contractile ring of AcGFP-tagged DIA1 proteins, respectively. Arrowheads indicate the enhanced phalloidin staining at the contractile ring. Scale bars: 10 μm. Representative of at least 3 experiments.

(A) AcGFP shows no accumulation at the spindle or contractile ring. Note the enhanced phalloidin staining at the contractile ring.

(B) AcGFP-DIA1 shows accumulation only at the spindle.

(C) AcGFP-DIA1(A265S) shows accumulation both at the spindle and contractile ring.

(D, E) AcGFP-DIA1(R1213X) shows accumulation both at the spindle and contractile ring (**D**), in contrast, AcGFP-DIA1(M1199D) shows accumulation only at the contractile ring (**E**). Both AcGFP-DIA1(R1213X) and AcGFP-DIA1(M1199D) show the plasma membrane localization (asterisks) in the metaphase, and asymmetric accumulation at the contractile ring (double arrows).

(F-G) Graphs demonstrates the percentage of AcGFP-positive cells showing asymmetrical asymmetric accumulation at the contractile ring (**F**, n = 4) and the percentage of AcGFP-positive floating and dead cells in the metaphase (**G**, n= 4), respectively. ****$P < 0.0001$, **$P = 0.0066$ (A265S vs. R1213X), and **$P = 0.0022$ (R1213X vs. M1199D) by one-way ANOVA followed by Tukey's *post hoc* test.

Supplementary information

Supplementary Fig. S1. Crystal structure of the DID/DAD interface.

(**A**) Surface representation of the DAD (PDB ID code 3o4x.1.D; A1191 to K1215) and the DID (PDB ID code 1z2c.1.B). (**B**) Residues M1199 (green), L1202 (dark red), and L1206 (blue) of the DAD (upper panel) bind with the residues A265 (pink), M225 (dark blue), I231 (solid red) and L262 (white) of the DID creating the autoinhibitory interaction between DID and DAD in DIA1-1 (lower panel). Protein sequence (NP_005210) and structures were analyzed by ExPASy (https://www.expasy.org/structural_bioinformatics) and the crystal 3D structures were created by ngl-tools (http://proteinformatics.charite.de/ngl-tools/ngl/html/ngl.html).

Supplementary Fig. S2. Normal platelet morphology from carriers of DIAPH1 p.A265S variant.

Peripheral blood smear staining of III:4 (F/5) (**A**) and II:1 (M/35) (**B**) shows normal sized platelet (black arrow). (**C**) Characteristics of blood cell phenotypes from two patients with the DIAPH1 variant (c.G793T:p.A265S): MPV, Mean Platelet Volume; PCT, Plateletcrit; PDW, Platelet Distribution Width; Hb, Hemoglobin; WBC, White Blood Cell; Seg.Neut., segmented neutrophil.

Supplementary Fig. S3. Variously impaired DID-DAD interaction by hypothetical mutants in the DID: p.I231T, p.I231R, p.L262T, p.L262E.

(**A**) Purified GST-tagged DID proteins (p.A265S, p.I231T, p.I231R, p.L262T, p.L262E, and p.E273R) were mixed with synthesized biotin-labeled WT DAD peptides in a binding buffer. After rotation, streptavidin-coupled magnetic beads were added to the solution, and the mixture was agitated. The materials absorbed to the beads were subjected to SDS-PAGE, followed by

immunoblotting using an HRP-conjugated GST antibody. Note the significantly diminished binding between DID(A265S), DID(I231T), DID(I231R), DID(L262T) and DID(L262E) and WT DAD, compared with that between DID(E273R) and WT DAD. Comparable levels of input (GST proteins) are shown in the left side of the panel (Representative of 7 experiments). (**B**) The DID-DAD interaction was quantified using an ImageJ software (n=7, ****$P < 0.0001$ by one-way ANOVA followed by Tukey's *post hoc* test).

Supplementary Fig. S4. PM localization and enhanced phalloidin staining in AcGFP-DIA1 mutants: constitutively active I231T, I231R, L262E, expressing HeLa cells.

AcGFP-DIA1(I231T), AcGFP-DIA1(I231R), AcGFP-DIA1(L262T), AcGFP-DIA1(L262E), and AcGFP-DIA1(E273R) were transfected into HeLa cells. Thirty hours after transfection, the cells were fixed and stained using Alexa568-conjugated phalloidin (red) and DAPI (blue). AcGFP-DIA1(I231T), AcGFP-DIA1(I231R), and AcGFP-DIA1(L262E), but not AcGFP-DIA1(L262T) or AcGFP-DIA1(E273R), show the weak plasma membrane (PM) localization (arrows) and enhanced phalloidin staining at the outlines of the cells (circles). Scale bars: 10 μm.

Supplementary Fig. S5. Accumulation of AcGFP-DIA1 mutants, I231T, I231R, L262E, at the contractile ring during cell division.

AcGFP-DIA1(I231T), AcGFP-DIA1(I231R), AcGFP-DIA1(L262T), AcGFP-DIA1(L262E), AcGFP-DIA1(E273R), and AcGFP-DIA1(A265S) were transfected into the HeLa cells. Thirty hours after transfection, the cells were fixed and stained using Alexa568-conjugated phalloidin (red) and DAPI (blue). Arrows and double arrows indicate accumulation of AcGFP-tagged DIA1 proteins at the spindle and contractile ring, respectively. Scale bars: 10 μm. Representative of 3 experiments.

(**A, D, F**) AcGFP-DIA1(I231T), AcGFP-DIA1(L262E), and AcGFP-DIA1(A265S) show accumulation of AcGFP-tagged DIA1 proteins both at the spindle and contractile ring. (**B**) AcGFP-DIA1(I231R) shows accumulation both at the spindle and contractile ring, but shows the strong plasma membrane localization (asterisks) in the metaphase. (**C, E**) AcGFP-DIA1(L262T) and AcGFP-DIA1(E273R) show accumulation at the spindle, but not contractile ring. (**G**) The cumulative bar graph shows the number of AcGFP (n=10), AcGFP-DIA1 (n=20), AcGFP-DIA1(A265S) (n=30), AcGFP-DIA1(R1213X) (n=20), AcGFP-DIA1(M1199D) (n=20), AcGFP-DIA1(I231T) (n=20), AcGFP-DIA1(I231R) (n=20), AcGFP-DIA1(L262T) (n=20), AcGFP-DIA1(L262E) (n=20), or AcGFP-DIA1(E273R) (n=20) expressing cells with (w) or without (wo) accumulation at the contractile ring. Data are obtained at 5 dishes from 3 experiments.

Supplementary Movies S1–S4: Single-molecule speckle (SiMS) microscopy of XTC cells expressing WT and mutants.

Time-lapse images of XTC cells expressing AcGFP-tagged DIA1(WT) (**S1**, representative video of 5 experiments), DIA1(A265S) (**S2**, representative video of 5 experiments), DIA1(R1213X) (**S3**, representative video of 4 experiments), DIA1(M1199D) (**S4**, representative video of 5 experiments) were acquired every 300ms. Circles indicate the speckles showing directional movement. Time is in seconds. Scale bars are 5 μm.

Table 1. Variant described in this study

Variant (*DIAPH1*) NM_005219	Global Minor Allele Frequency (MAF)				Ethinicity-specific MAF	Conservation Score		Prediction Algorithm		Functional Study (This study)	Classification [22 23]
	1000G	ExAC	GO-ESP	gnomAD	KRGDB	PhyloP	GERP++	CADD	REVEL	Significantly impaired autoinhibitory interaction	**Likely Pathogenic** (PS3 supporting, PM2 moderate, PP1 supporting, PP3)
c.793G>T: p.A265S	absent	absent	absent	absent	absent	5.909	5.69	27.4	0.786	Abnormally upregulated actin polymerization activity	

1000G, 1000 Genomes (https://www.ncbi.nlm.nih.gov/variation/tools/1000genomes/); ExAC, Exome Aggregation Consortium (http://exac.broadinstitute.org/); GO-ESP, NHLBI Grand Opportunity Exome Sequencing Project (https://esp.gs.washington.edu/drupal/); gnomAD, genome aggregation database (http://gnomad.broadinstitute.org/); KRGDB, Korean Reference Genome DB (http://152.99.75.168/KRGDB/); PhyloP score from the Mutation Taster (http://www.mutationtaster.org/); GERP++ score in the UCSC Genome Browser (http://genome-asia.ucsc.edu/); CADD, Combined Annotation Dependent Depletion (https://cadd.gs.washington.edu/snv); REVEL, Rare Exome Variant Ensemble Learner (https://sites.google.com/site/revelgenomics/).

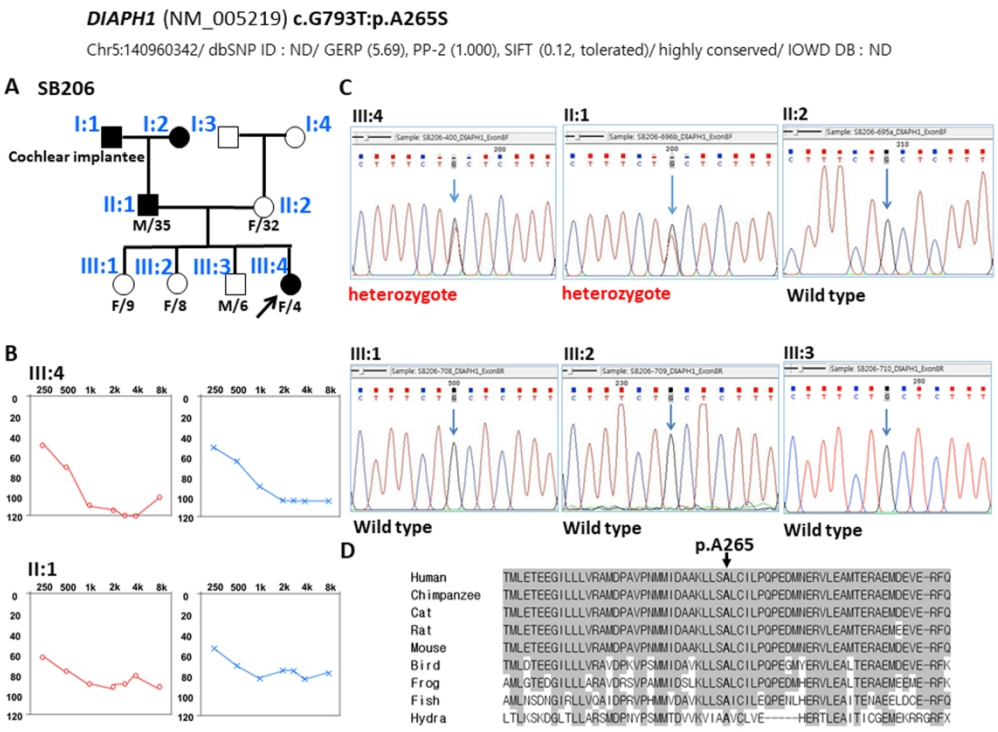


Figure 1

254x190mm (300 x 300 DPI)

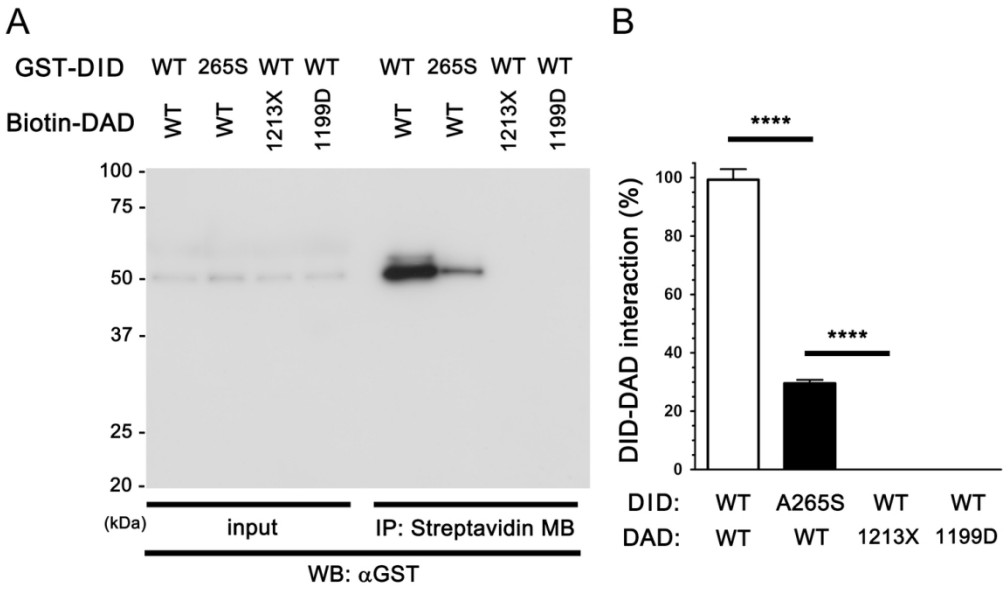


Figure 2

128x74mm (300 x 300 DPI)

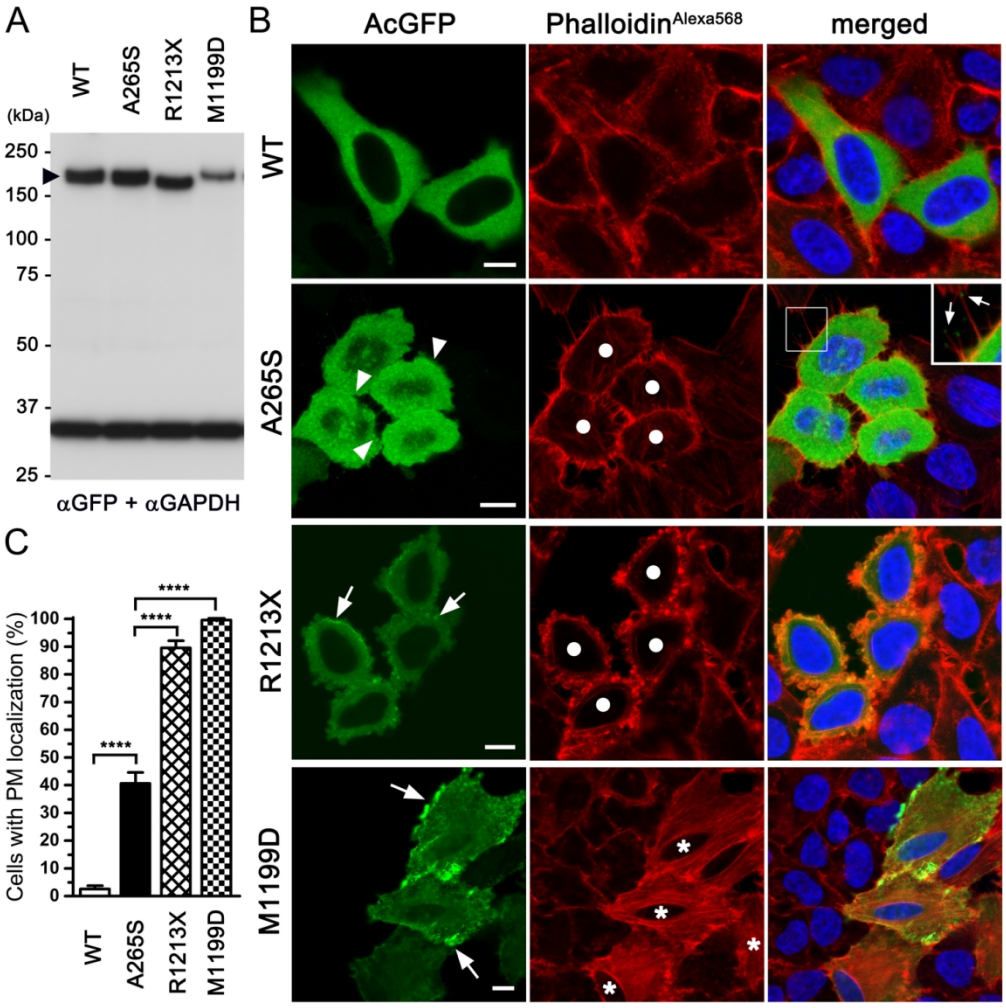


Figure 3

128x127mm (300 x 300 DPI)

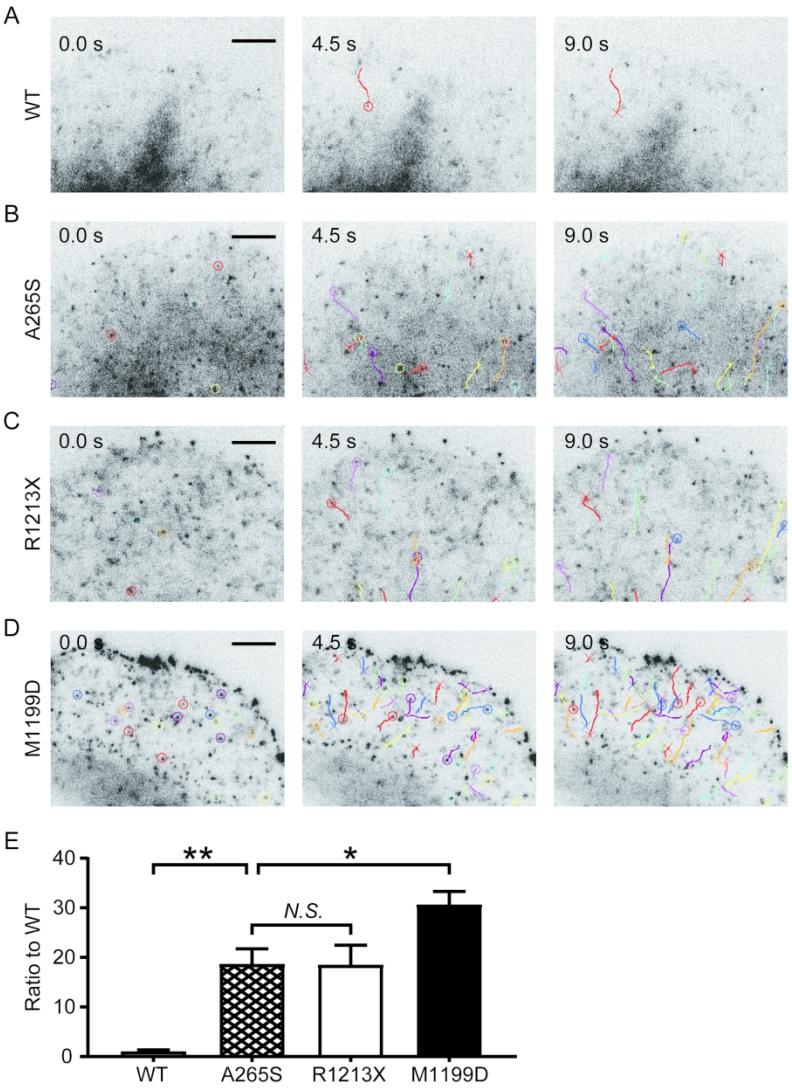

A
WT
0.0 s
4.5 s
9.0 s
B
A265S
0.0 s
4.5 s
9.0 s
C
R1213X
0.0 s
4.5 s
9.0 s
D
M1199D
0.0 s
4.5 s
9.0 s
E
Ratio to WT
40
30
20
10
0
**
*
N.S.
WT
A265S
R1213X
M1199D

Figure 4

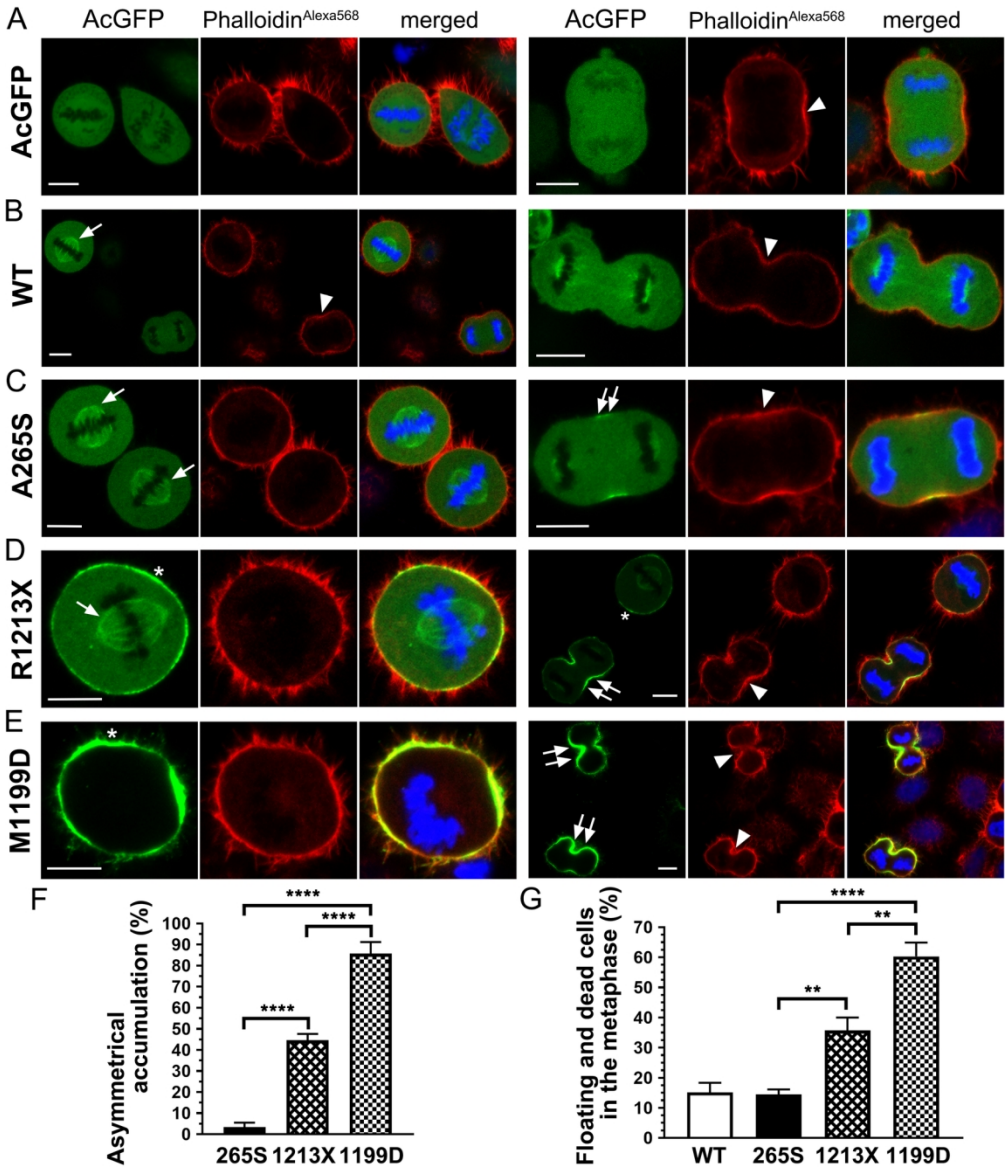


Figure 5

150x174mm (300 x 300 DPI)

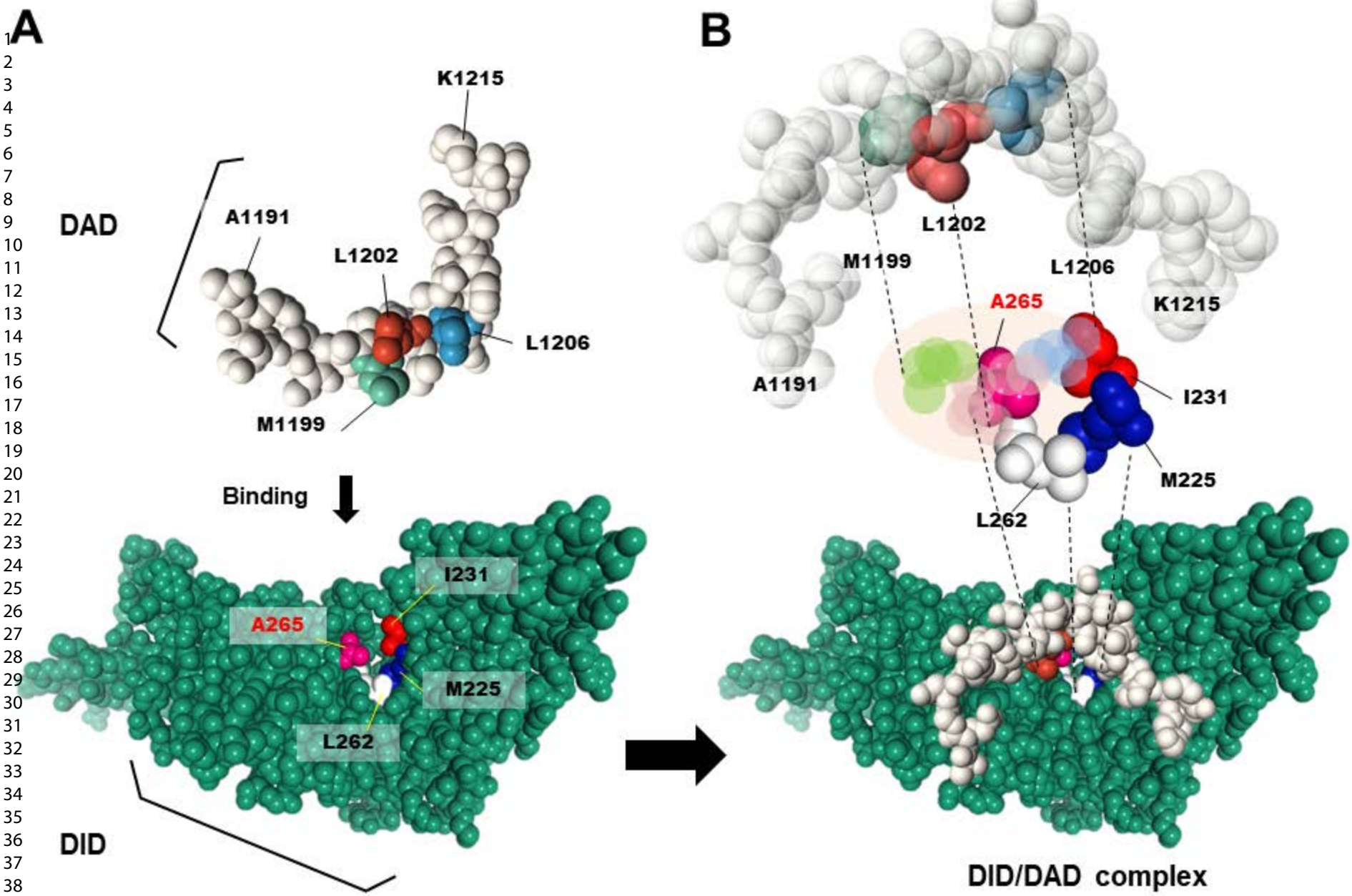
Supplementary Table S1. Variants that survived initial basic filtering after targeted exome sequencing of 149 deafness genes

Gene	Chr	GenbankID	Exon	Nucleotide Change	Amino Acid Change	Pathogenicity Prediction			Zygosity
						SIFT	Polyphen2	Mutation Taster	
ITPKB	chr1	NM_002221	exon8	c.A2753T	p.E918V	T	P	D	hetero
DIAPH1	**chr5**	**NM_001079812,NM_001314007, NM_005219**	**exon7,exon8,exon8**	**c.G766T,c.G793T,c.G793T**	**p.A256S,p.A265S,p.A265S**	**T**	**D**	**D**	**hetero**
SLC26A5	chr7	NM_001167962,NM_198999, NM_206883	exon14,exon15,exon15	c.G1477A,c.G1573A,c.G1573A	p.A493T,p.A525T,p.A525T	T	D	D	hetero
GARNL3	chr9	NM_032293,NM_001286779	exon21,exon22	c.C1957A,c.C1891A	p.P653T,p.P631T	.	D	D	hetero
KCNQ1	chr11	NM_000218	exon1	c.G46A	p.G16S	T	B	D	hetero
KCNQ1	chr11	NM_000218	exon1	c.C68T	p.A23V	D	B	D	hetero
OTOGL	chr12	NM_173591	exon46	c.C5702T	p.T1901M	T	.	N	hetero
TBC1D24	chr16	NM_020705,NM_001199107	exon7,exon8	c.C1552T,c.C1570T	p.R518W,p.R524W	T	B	D	hetero
MYO15A	chr17	NM_016239	exon56	c.C9478T	p.L3160F	D	D	D	hetero
FLII	chr17	NM_001256265,NM_001256264, NM_002018	exon20,exon21,exon21	c.G2378T,c.G2510T,c.G2543T	p.R793L,p.R837L,p.R848L	D	D	D	hetero
MAP2K3	chr17	NM_002756,NM_145109, NM_001316332	exon11,exon11,exon12	c.G855T,c.G942T,c.G855T	p.M285I,p.M314I,p.M285I	D	B	D	hetero
LOXHD1	chr18	NM_001308013,NM_001145472, NM_144612	exon7,exon9,exon27	c.A526G,c.A814G,c.A4147G	p.T176A,p.T272A,p.T1383A	T	P	N	hetero
GRIN3B	chr19	NM_138690	exon9	c.C2794G	p.R932G	T	P	D	hetero
TSPEAR	chr21	NM_144991,NM_001272037	exon3,exon4	c.C442T,c.C238T	p.R148C,p.R80C	D	D	D	hetero

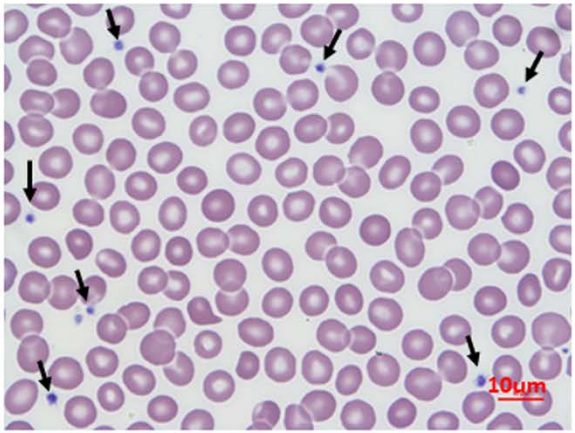
T: Tolerated, P: Probably damaging, D: Damaging, B: Benign, N: Neutral

SIFT (http://sift.jcvi.org/); Polyphen-2 (http://genetics.bwh.harvard.edu/pph2/); Mutation Taster (http://www.mutationtaster.org/)

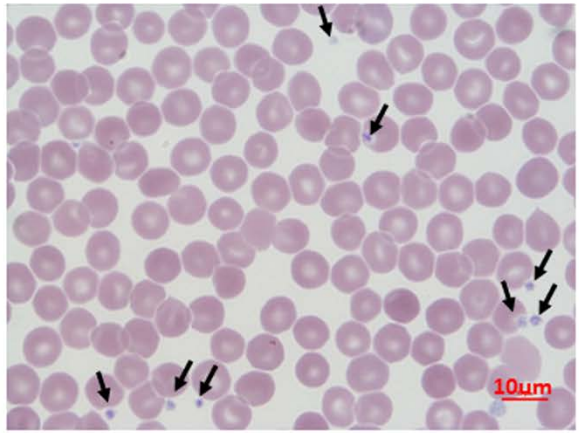
Confidential: For Review Only


A
DAD
K1215
A1191
L1202
L1206
M1199
Binding
I231
A265
M225
L262
DID
B
L1202
M1199
L1206
K1215
A265
A1191
I231
M225
L262
DID/DAD complex

A

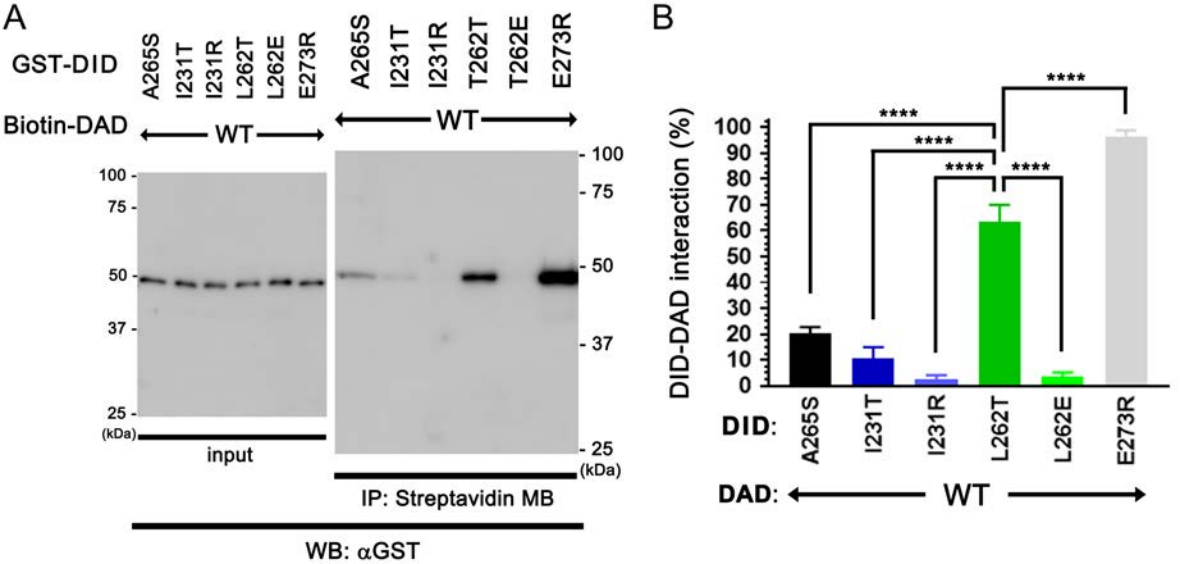


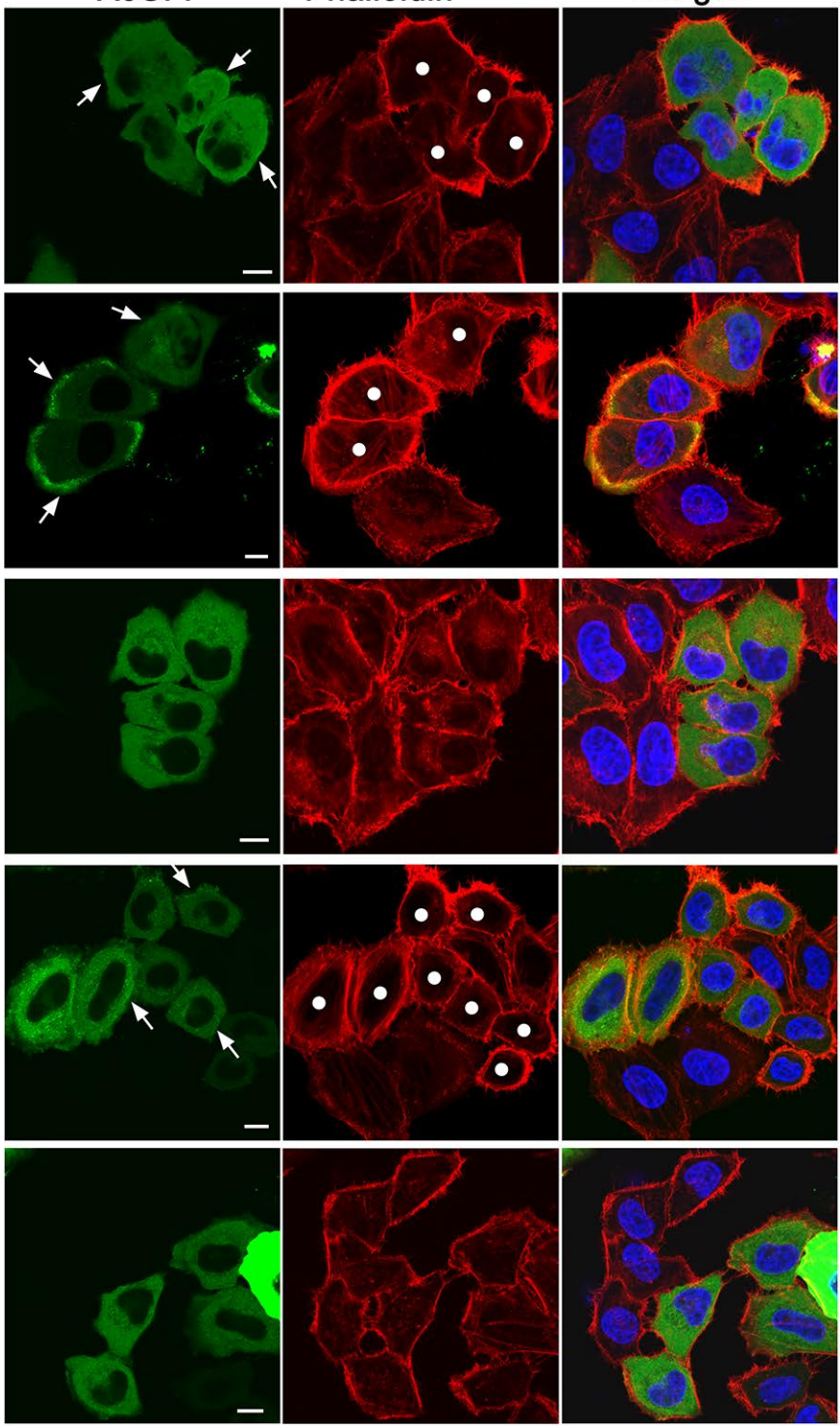
B

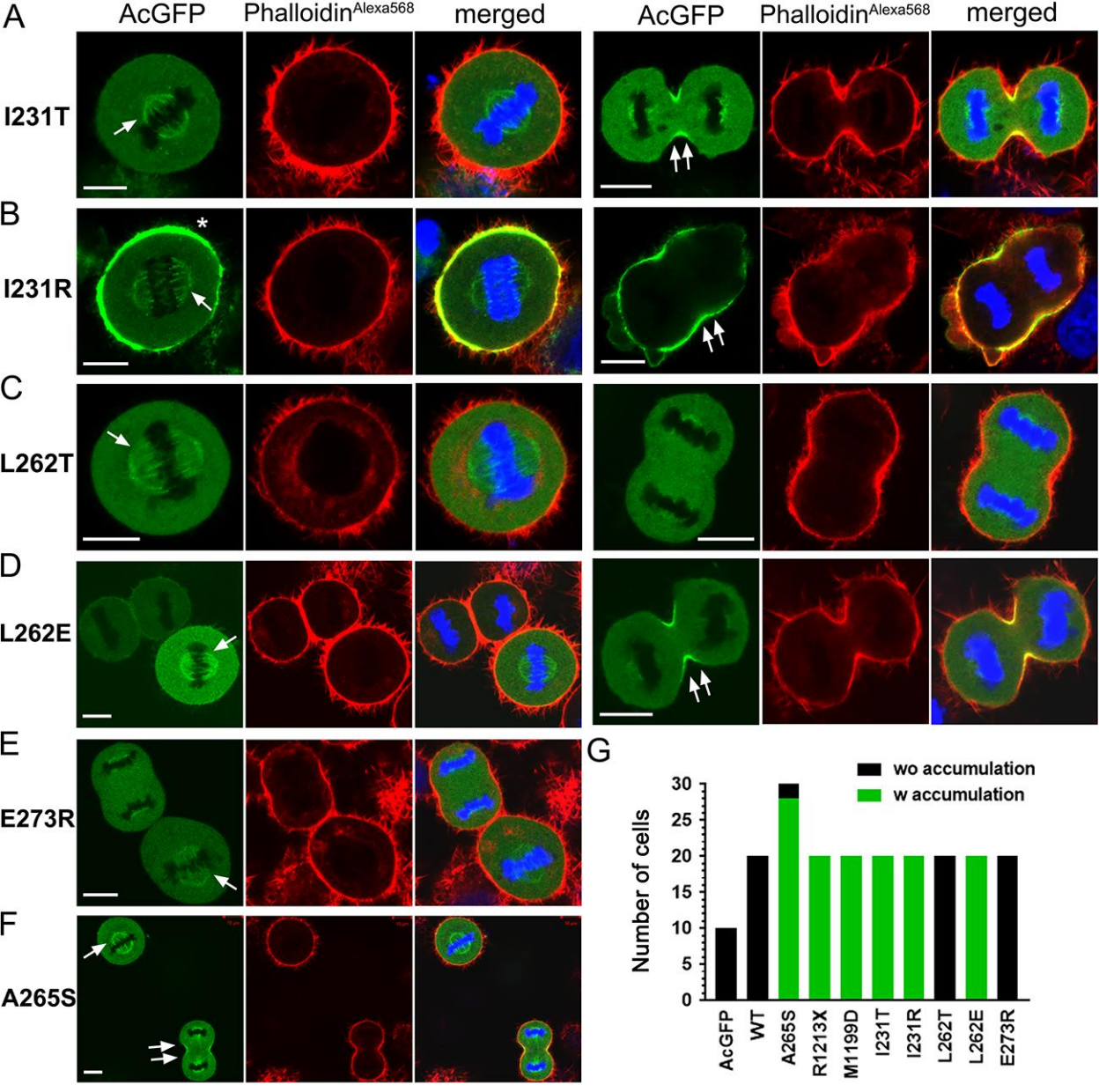


C

Patient	Age (yr) Gender	Platelet count, 10^3/ul (130-400)	MPV, fL (7.4-10.4)	PCT, % (0.15-0.32)	PDW, fL (15.5-17.5)	Hb, g/dL	WBC, 10^3/ul (4.0-10.0)	Seg. Neut., % (50-75)
III:4	3 (F)	272	9.9	0.27	11.7	15.1 (12-16)	10.24	42.1
	5 (F)	346	9.3	0.32	10.7	14.8 (12-16)	10.27	57.0
II:1	35 (M)	251	8.7	0.22	10.3	16.3 (13-17)	8.48	58.9


A
GST-DID
A265S
I231T
I231R
L262T
L262E
E273R
A265S
I231T
I231R
T262T
T262E
E273R
Biotin-DAD
WT
WT
100
75
50
37
25
(kDa)
input
IP: Streptavidin MB
WB: αGST
B
DID-DAD interaction (%)
****
DID:
DAD:
WT


AcGFP
Phalloidin Alexa568
merged
I231T
I231R
L262T
L262E
E273R


A
AcGFP
Phalloidin Alexa568
merged
AcGFP
Phalloidin Alexa568
merged
I231T
B
I231R
C
L262T
D
L262E
E
E273R
F
A265S
G
wo accumulation
w accumulation
Number of cells
30
25
20
15
10
5
0
AcGFP
WT
A265S
R1213X
M1199D
I231T
I231R
L262T
L262E
E273R